

# **LONG-TERM BENDING STRESS RELAXATION IN BENT GLUED LAMINATED TIMBER BEAMS**

## **LANGZEIT-RELAXATION DER BIEGESPANNUNG IN GEBOGENEN BRETTSCHICHTHOLZTRÄGERN**

Dominique Streib, Mohsen Naghdinasab, Aaron Münzer, Gerhard Dill-Langer  
*Materials Testing Institute (MPA), University of Stuttgart, Otto-Graf-Institute*

### **SUMMARY**

This article presents the results of long-term relaxation tests performed on glued laminated timber (GLT) beams. Initially straight beams were bent with two different radii over a period of 38 months, with the temporal development of reaction force being continuously recorded. These long-term experiments were conducted in service class 2 to investigate the impact of temperature and moisture variations on relaxation behaviour. In addition, a set of short-term and long-term numerical simulations was carried out using the experimental start and boundary conditions to reproduce the rheological response of the beams.

### **ZUSAMMENFASSUNG**

Dieser Artikel präsentiert die Ergebnisse von Langzeit-Relaxationsversuchen an Brettschichtholzträgern. Dazu wurden über einen Zeitraum von 38 Monaten ursprünglich gerade Träger mit zwei unterschiedlichen Radien gebogen und die dabei auftretende zeitliche Entwicklung der Reaktionskraft kontinuierlich aufgezeichnet. Die Versuche wurden in Nutzungsklasse 2 durchgeführt, um den Einfluss von Temperatur- und Feuchteänderungen auf das Relaxationsverhalten zu untersuchen. Zusätzlich wurde eine Reihe von numerischen Kurz- und Langzeitsimulationen unter der Verwendung der experimentellen Anfangs- und Randbedingungen durchgeführt, um die rheologische Reaktion der Biegeträger zu modellieren.

# 1. INTRODUCTION

Timber lattice shells as highly efficient structural timber structures can be produced by elastically curving of initially straight timber elements. The forming process in this case generates high initial bending stresses that can potentially overstress the timber elements under service loads [1]. Nevertheless, due to the rheological behaviour of wood which (under constant deformation) results in stress relaxation, these initial stresses are usually assumed to decrease over time to acceptable levels.

However, long-term bending stress relaxation of lattice timber elements are not investigated appropriately and the available short-term studies are inapplicable to structural design. In this regard, some approaches such as ‘bending stress reduction approach’ and ‘bending strength reduction approach’ try to address this structural design challenge [2, 3]. However, these methods either are valid only for short-term, or neglect the residual bending stresses that play a significant role in overall stability of such analyses in long-term. Therefore, accurate long-term investigation of stress relaxation in pure bending of practical structural elements is needed.

## 1.1 *Project description*

The long-term experiments discussed in this article were part of a test series conducted at the Materials Testing Institute (MPA) of the University of Stuttgart for the construction of the new elephant house in the zoological-botanical garden in Stuttgart. At the end of 2024, the state parliament approved the construction of the planned "Elefantenwelt" with costs estimated at approximately 68.5 million euros. Construction is scheduled to begin in October 2025 [4]. The client is the State of Baden-Württemberg, represented by Vermögen & Bau Baden-Württemberg.

The roof structure of the elephant house was designed as a timber lattice shell. The MPA was commissioned to conduct stiffness tests on the timber lattice shell nodes. A detailed description of the project and the experimental test series was already summarized in the Otto-Graf-Journal in 2022 [5]. The roof structure, conceived as an arch structure, consists of a primary and a secondary load-bearing direction. The primary direction is spanned by glued laminated timber (GLT) beams of strength class GL 28h acc. to EN 14080 [6] with cross-sectional dimensions  $w \times h = 24 \text{ cm} \times 32 \text{ cm}$  over the shorter span, while the secondary direction

consists of GL 28h beams with a cross-section of  $w \times h = 24 \text{ cm} \times 12 \text{ cm}$ , which are responsible for load transfer and stabilization of the shell structure. The beams in the secondary load-bearing direction are to be manufactured as straight GLT beams and subsequently installed on-site into their predefined curvature.

To assess the relaxation behaviour due to the rheological properties of timber, long-term investigations were carried out with GLT beams in a service class 2 environment from April 2022 to July 2025, which will be reported on in the following.

## **1.2 Rheological background of wood**

Creep and relaxation are manifestations of the same fundamentally time-dependent (rheological) behaviour of wood as a material. These two phenomena have to be accounted for in engineering and structural calculations. Thereby, the rheological behaviour of wood and timber products is not only governed by pure time dependency (“viscoelastic” behaviour), but also by special interactions between loads and varying moisture contents (the so-called “mechano-sorptive” effects [7]). During the sorption and desorption cycles, e. g. caused by seasonal changes, this phenomenon accelerates the overall strain significantly compared to purely viscoelastic deformations [8]. In fact, the mechano-sorptive behaviour plays a decisive role in the long-term performance of structural timber elements i. a. by changing their internal stress distribution.

Most studies and standards have addressed the rheological behaviour of wood with a specific focus on creep [9]. However, also relaxation phenomena are of interest, as they could act as beneficial from a structural analysis point of view and results in a partial recovery of the structural elements [10]. Current structural design standards often include verified data and analyses for creep, while the long-term structural analyses for stress relaxation are generally absent. The lack of long-term experimental campaigns and established analyses for stress relaxation may result in structural design uncertainties for the usage of grid shell elements under constant deformation. Besides, multi-layered timber elements such as lattice shells and grid shells that are produced on-site by bending initially straight beams are subjected to high bending stresses that may exceed their permissible levels [3]. These problems should be addressed appropriately to increase the applicability of such structural elements in real construction.

## 2. TEST SET-UP

The raw material for the experimental campaign was four GLT beams of strength class GL 28h made from Norway spruce (*Picea abies*) laminations and dimensions  $w \times h \times l = 140 \text{ mm} \times 120 \text{ mm} \times 12 \text{ m}$ . The strength and stiffness values of the beams are declared according to EN 14080 [6].

The beams were cut at half length, resulting in eight beams with lengths of 5.94 m each. A simple test setup requiring minimal technical equipment and auxiliary means was developed. Each test setup comprised two beam parts, termed A and B in the following. The test beams were positioned and consequently bent around their weak axis, i.e., with vertically oriented lamellas. At the beam ends, two steel plates and a steel roll acted as hinged supports. At mid-length of the beams, steel plates and a compression load cell with a capacity of 50 kN were installed. The height of this construction was chosen according to the mid-deflection target and the approximate bending radius. At the ends of the beams, the two initially straight GLT beams were then braced together with steel U-beams and threaded rods until contact to the steel roll was achieved. Thereby, the desired deflection was achieved. In total, four test setups were installed - two with a mid-span deflection of  $u_1 = 83.28 \text{ mm}$  and an approximate bending radius of  $R_{\min} = 53 \text{ m}$  (442 h), and two with a mid-span deflection of  $u_2 = 61.28 \text{ mm}$  and an approximate bending radius of  $R_{\max} = 72 \text{ m}$  (600 h). The load cells continuously recorded the bending process from the start of loading. Fig. 1 schematically illustrates the structural configuration of a test specimen, exemplified by an approximate curvature radius of  $R_{\min} = 53 \text{ m}$ . Fig. 2 shows a photo of all specimens that underwent long-term testing.

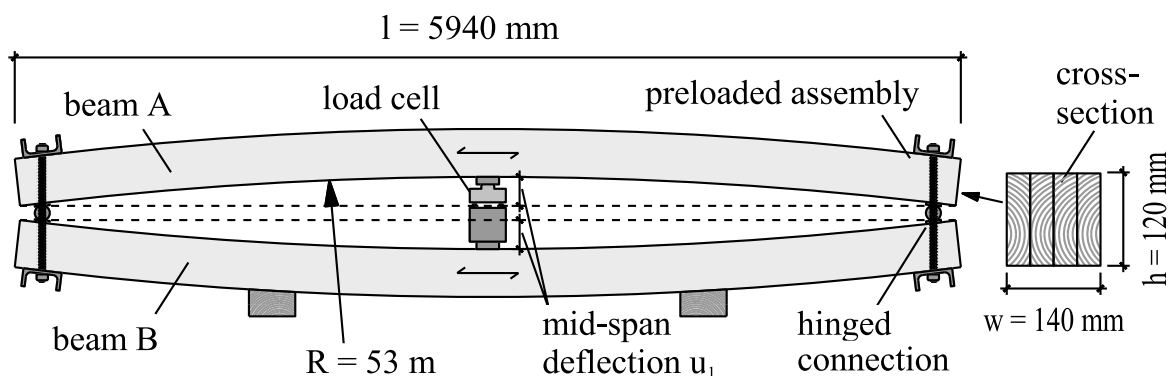


Fig. 1: Schematic drawing of the test setup (not to scale)

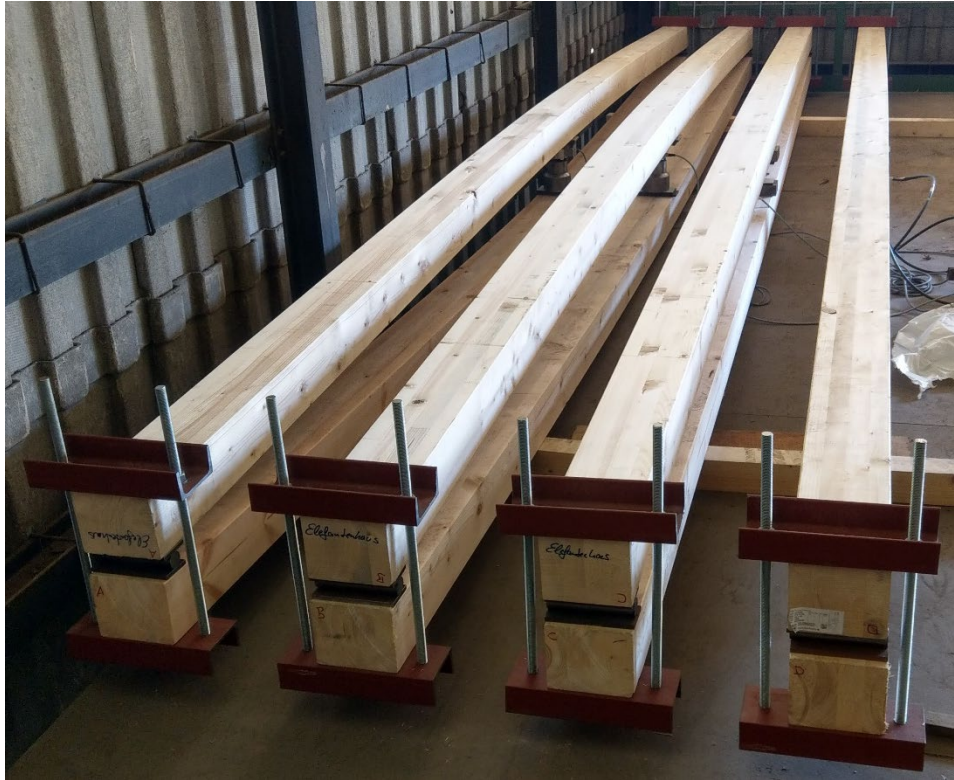


Fig. 2: Photo of the four specimens during the long-term test

The test setups were placed in an unheated, naturally ventilated testing hall. The beams were protected from direct exposure to weather conditions, but exposed to outdoor temperature and relative humidity. This scenario corresponds to service class 2 acc. to EN 1995-1-1 [9]. The ambient temperature and the relative humidity in the hall were continuously recorded during the test period at a constant interval of 30 min. The moisture content of the GLT beams was monitored in the first months by means of an electrical measurement device. At the start of the experimental program, the beams were at approximately 12 % moisture. Table 1 summarizes all relevant properties for the four specimens.

Table 1: The geometric, strength and stiffness properties of the four test specimens

Specimen	Cross-section $w \times h$ [mm]	Strength class	Char. bending strength $f_{m,g,k}$ [N/mm <sup>2</sup> ]	Mean modulus of elasticity $E_{0,g,mean}$ [N/mm <sup>2</sup> ]	Applied mid-span deflection $u$ [mm]	Approximated bending radius $R$ [m]
F1	140 × 120	GL 28h	28	12.600	83.28	53
F2					83.28	53
F3					61.28	72
F4					61.28	72

Over a period of more than 38 months, the GLT beams were held under constant mid-span deflection within the test setup. From the start of the test in April 2022 until the end of November 2023, force measurements were recorded daily. After this period, no datasets are available due to the unavailability of the data acquisition system for the long-term test. Further measurements were then recorded in February, March and July 2025.

### 3. TEST RESULTS

Fig. 3 illustrates the evolution of the four measured forces during the first 44 hours of the long-term test. As depicted in Fig. 3, the test specimens were sequentially activated in a continuous, time-lagged manner, commencing with the structural members exhibiting the mid-span deflection of  $u_1 = 83.28$  mm. After approximately 21 hours, the final two specimens with the target mid-span deflection of  $u_2 = 61.28$  mm were subjected to the applied deformation. In all four specimens, it is evident that the force developing during the closing at the supports of the double-beam assemblies increases depending on the imposed curvature. Each individual force reaches its maximum at the beginning of the actual test and can be taken as the linear elastic reaction of the system. The differences of the maximum forces between the specimens with the same deflection result presumably from different individual stiffnesses.

Upon reaching the peak value, a virtually immediate reduction in force occurs for each specimen. This phenomenon is commonly referred to as instantaneous relaxation. After a certain period from the start of each test, the force progression levels off and continues with a slight slope, and some small fluctuations. For specimens F2, F3, and F4, the measurement value was selected after 3.33 minutes. For specimen F1, a constant slope of the curve - and thus a representative value for the relaxation restraint following the initial instantaneous relaxation - was identified from 7.5 minutes onwards.

The recorded force values are summarized in Table 2. The observed reduction in force after the few minutes mentioned amounts to 94 % (F1), 90 % (F2), 89 % (F3) and 82 % (F4).

After 24 hours the reductions were 85 % (F1), 81 % (F2), 85 % (F3) and 78 % (F4).

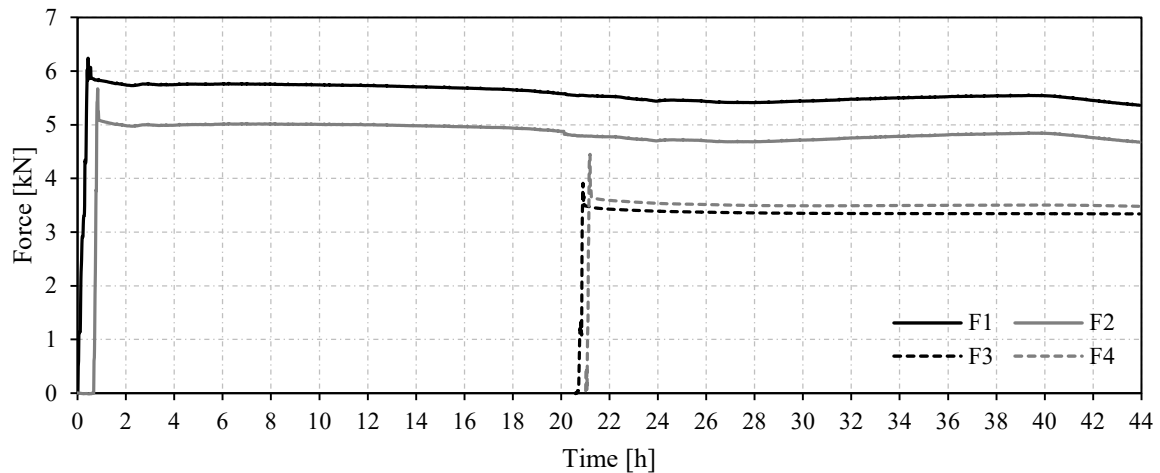


Fig. 3: Force-time diagram of the relaxation test during the initial 44-hour period

Table 2: Selected force values for the first hours of the long-term test

Specimen	Initial maximum. Load $F_0$ [kN]	Instantaneous relaxed load $F_{inst}$ [kN]	The time span for which relaxa- tion occurs instantaneously [min]
F1	6.24	5.87	7.50
F2	5.67	5.09	3.33
F3	3.91	3.50	3.33
F4	4.45	3.65	3.33

Figs. 4 and 5 depict the progression of the force  $F_t$  over the entire 38-month period for the four specimens, with the deflection and thus the approximate bending radii kept constant throughout. Additionally, the measured ambient temperature in the unheated, naturally ventilated hall (see Fig. 4, right vertical axis) and the relative humidity (see Fig. 5) are shown. The temperature and relative humidity each show strongly fluctuating curves when recorded at one value per day, as illustrated by the gray curves. The black curve represents a moving average calculated over 15 days.

A continuous slight decrease in the forces over time can be observed. Additionally, the climatic influence due to changing relative humidity is strongly evident in the force curves. A cyclic behaviour can be observed in the force curve for all four test specimens: During periods with increasingly dry and warm climate (spring to summer) the reaction force curves exhibit a decline, followed by a subsequent rise during more wet and cold periods in autumn and winter. The net effect of a complete seasonal cycle yields progressive decrease of the reaction loads.

Fig. 6 shows the time dependant relative reaction force level ( $F_t/F_0$ ) over the entire period for all four specimens. The ratio  $F_t/F_0$ , i.e., the reaction force normalised by the individual stiffnesses, shows qualitatively the same behaviour as the individual reaction force data: A continuous decreases throughout the entire testing period is observed, accompanied by the cyclic influence of the seasonal moisture and temperature changes. To determine an initial stress relaxation ratio, the first maximum force value is compared with the last measured value. This comparison yields ratios of 50 % and 52 % for the mid-span deflection of  $u_1 = 83.28$  mm as well as 48 % and 60 % for the mid-span deflection of  $u_2 = 61.28$  mm. To focus exclusively on long-term relaxation processes, the instantaneous relaxation is excluded, resulting in a stress relaxation ratio of 55 % and 56 % for the mid-span deflection of  $u_1 = 83.28$  mm as well as 58 % and 67 % for the mid-span deflection of  $u_2 = 61.28$  mm. However, in this analysis, a first value measured in April 2022 was compared with a last value measured in July 2025, i.e. some seasonal influence is incorporated.

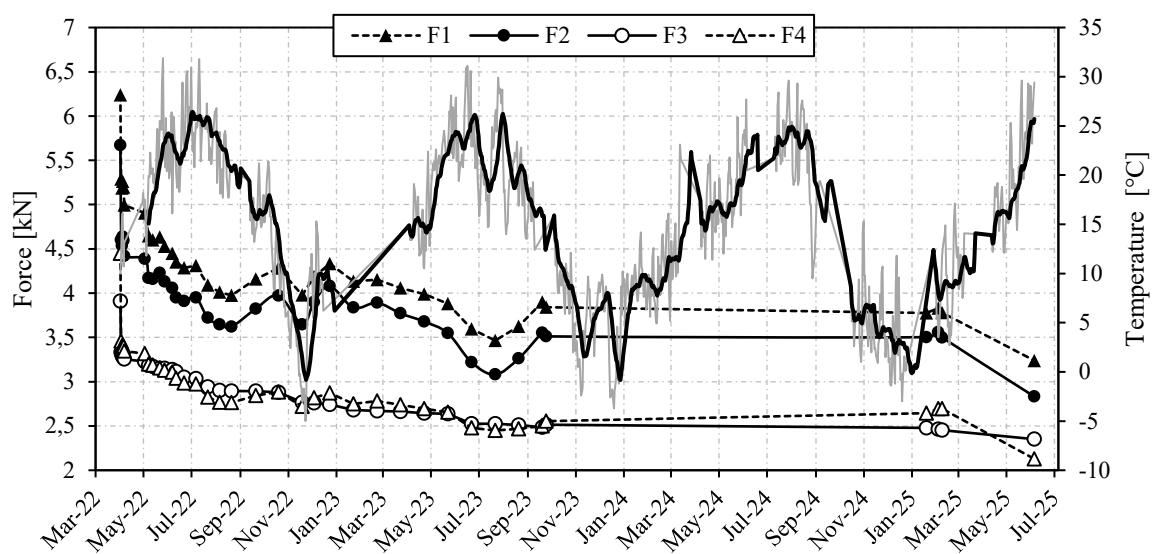


Fig. 4: Progression of the force  $F_t$  over the entire 38-month period and the ambient temperature

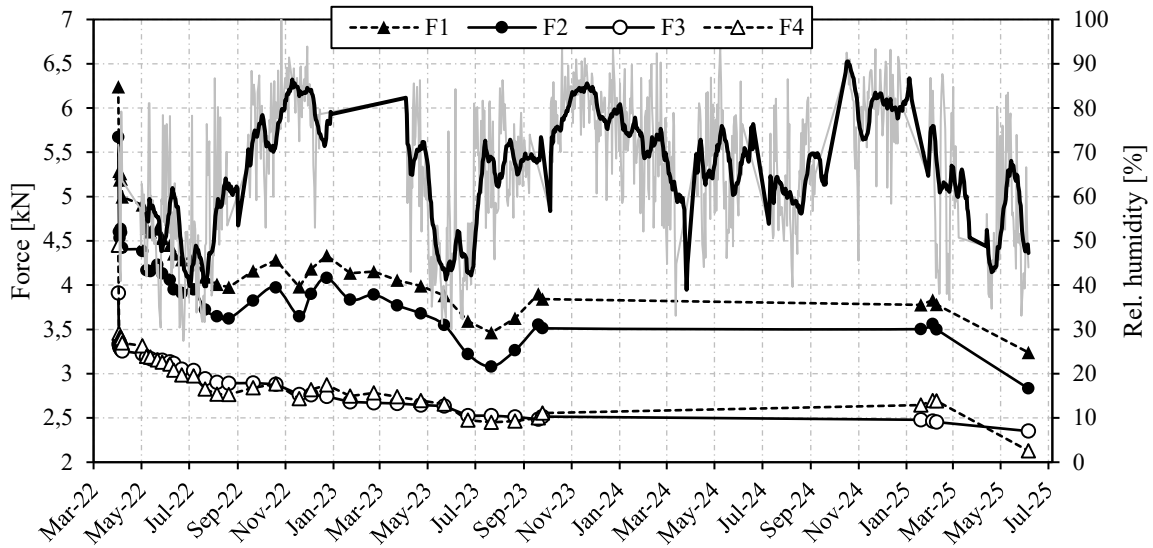


Fig. 5: Progression of the force  $F_t$  over the entire 38-month period and the and relative humidity

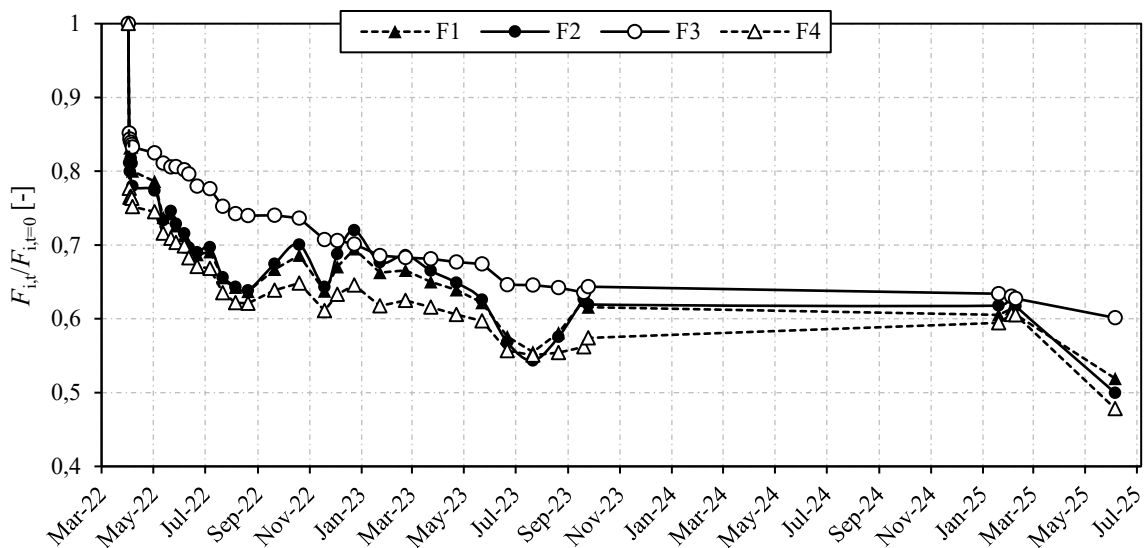


Fig. 6: Bending stress relaxation curve  $f(t)$ , which is represented by the force ratio ( $F_t/F_0$ )

For a more accurate assessment of stress reduction due to relaxation, it is necessary to make comparisons of equivalent values across analogous periods. Fig. 7 presents the force values for each specimen displayed at the 2<sup>nd</sup> of July in 2022, 2023, and 2025, respectively. A stress relaxation ratio of 27 % and 30 % for the mid-span deflection of  $u_1 = 83.28$  mm as well as 24 % and 32 % for the mid-span deflection of  $u_2 = 61.28$  mm is observed under these comparable conditions. This largely corresponds to the results of another study in which individual laths made of Eucalyptus globulus L. wood were bent into a constant shape over a two-year period [1].

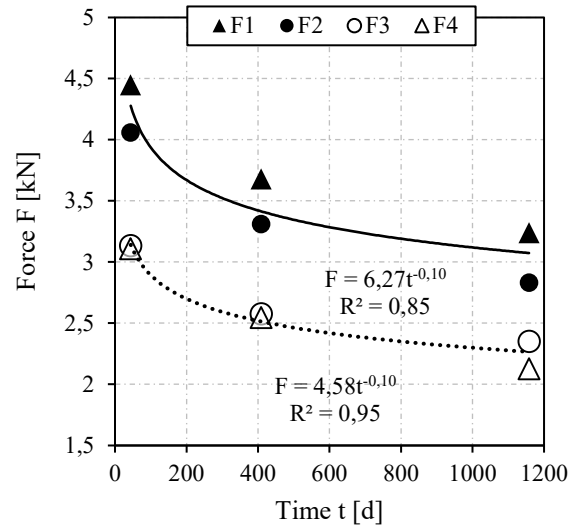


Fig. 7: Force values of all specimens measured on 2<sup>nd</sup> of July 2022, 2023 and 2025 at comparable ambient conditions

Assuming a simply supported, single-span beam, the induced bending stress in each GLT beam can be determined. This can be modelled by considering an external load acting in the middle due to the applied curvature. Table 3 shows the  $F_t/F_0$  ratio and the calculated induced stresses at mid-span for all four beams. Values are given for time points of  $t_1 =$  one day,  $t_7 =$  one week,  $t_{14} =$  two weeks,  $t_{28} =$  one month,  $t_{180} =$  six months,  $t_{365} =$  one year and  $t_{1160} =$  38 months.

Table 3:  $F_t/F_0$  ratio and the calculated induced stresses in  $N/mm^2$  at mid-span

Date	Parameters	Specimen			
		F1	F2	F3	F4
$t = 0$	$F_t/F_0$	1	1	1	1
	$\sigma_{t=0}$	16.1	14.6	10.1	11.5
$t_1 =$ one day	$F_t/F_0$	0.848	0.811	0.852	0.778
	$\sigma_{t=1}$	13.6	11.9	8.59	8.92
$t_7 =$ one week	$F_t/F_0$	0.809	0.797	0.829	0.755
	$\sigma_{t=7}$	13.0	11.7	8.35	8.66
$t_{14} =$ two weeks	$F_t/F_0$	0.745	0.735	0.813	0.719
	$\sigma_{t=14}$	12.0	10.8	8.20	8.25
$t_{28} =$ one month	$F_t/F_0$	0.737	0.733	0.811	0.716
	$\sigma_{t=28}$	11.87	10.71	8.19	8.23
$t_{180} =$ six months	$F_t/F_0$	0.686	0.7	0.737	0.649
	$\sigma_{t=180}$	11.0	10.2	7.43	7.45
$t_{365} =$ one year	$F_t/F_0$	0.639	0.649	0.678	0.607
	$\sigma_{t=365}$	10.3	9.49	6.83	6.96
$t_{1160} =$ 38 months	$F_t/F_0$	0.519	0.499	0.601	0.479
	$\sigma_{t=1160}$	8.35	7.30	6.06	5.49

The maximum stress, as determined at time  $t = 0$  for test specimen F1, was found to be  $\sigma_{t=0} = 16.1 \text{ N/mm}^2$ , which is equivalent to 57 % of the characteristic bending stress of GL28h. Following the termination of the test, a substantial reduction in internal stresses is observed, reaching 30 % of the characteristic value.

On July 2<sup>nd</sup> 2025, the loading device (i.e. the forced deformation) was released, resulting in the unloading of the beams. Following this release, the previously straight glued laminated timber beams exhibited residual deformations. These deformations were recorded immediately after the termination of the test on 2<sup>nd</sup> of July 2025, after about two months on 1<sup>st</sup> of September 2025 and again three months after unloading at 2<sup>nd</sup> of October 2025. Table 4 compiles the measured deformations of the respective specimens at the aforementioned time points. The deflections were determined on both beams A and B of each test specimen. In order to ensure direct comparability of the results with the condition during the test, the constant mid-span deflections applied to the individual beams during the long-term test are given for comparison. Upon unloading of the specimens, average residual deflections of 30.1 and 24.4 mm were observed for  $R_{\min} = 53 \text{ m}$  (F1 and F2) and  $R_{\max} = 72 \text{ m}$  (F3 and F4), respectively, which correspond to 36 % and 40 % of the nominal mid-span deflection applied throughout the test period. It can be noted that these values correspond well to the overall force/stress reduction  $F_{t=1160}/F_{t=1}$  across all specimens ranging between 29 and 39 % and averaging 36 % at the end of the test period.

*Table 4 Residual mid-span deflections measured after the long-term test was completed*

Specimen	Part	Nominal mid-span deflection $u$ during long-term-test [mm]	Residual mid-span deflection [mm] on		
			07/02/2025	09/01/2025	10/02/2025
F1	A	83.28	29.0	23.7	17.7
	B	83.28	26.1	20.9	14.7
F2	A	83.28	36.7	31.0	24.1
	B	83.28	28.5	22.5	18.3
F3	A	61.28	17.5	15.1	12.8
	B	61.28	29.0	25.7	20.2
F4	A	61.28	27.4	24.1	17.1
	B	61.28	23.5	20.0	16.2

## 4. MODELING

As a supplementary for the experimental results, numerical simulations were also implemented to investigate the long-term relaxation behaviour of tested beams in presence of hygroscopic effects of moisture contents changes during the testing period.

For the numerical analysis of the forces in the GLT beams over the period of tests run, ABAQUS FEA 2022 was employed together with a 3D orthotropic material model defined in a UMAT subroutine. This model (demonstrated in Fig. 8), previously validated and verified, includes all instantaneous and long-term deformation behaviours as part of a hygro-mechanical constitutive description [11].

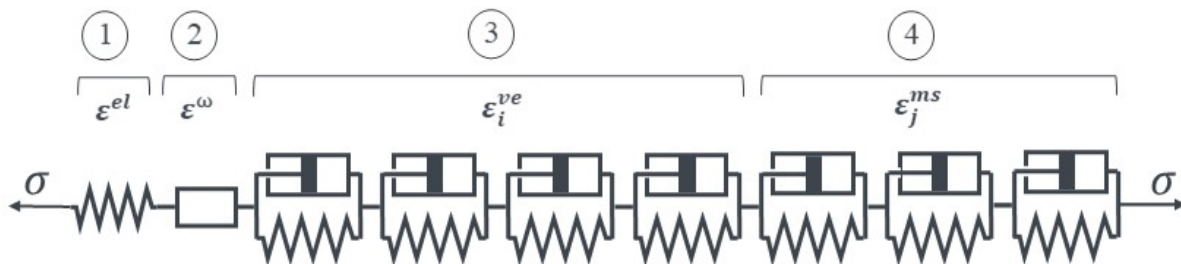


Fig. 8: Material model made of (1) one elastic element, (2) one hygro-expansion element, (3) four viscoelastic Kelvin-Voigt elements and (4) three mechano-sorptive Kelvin-Voigt elements

This material model uses rheological elements combined in series including elasticity ( $\varepsilon^{el}$ ), hygro-expansion ( $\varepsilon^{\omega}$ ), viscoelasticity ( $\varepsilon_i^{ve}$ ), and mechano-sorption ( $\varepsilon_j^{ms}$ ). Using this model ensures that all known deformation mechanisms in wood are represented to accurately capture the load-dependent and moisture-dependent relaxation in tested samples. The model parameters as e.g., spring constants and dashpot times of all Kelvin-Voigt elements, mechano-sorptive coefficients etc. have been used solely according to the values given in [10] for the wood species Norway spruce without any fit or adjustments with respect to the empiric test result data.

### 4.1 Model Geometry and Applied Boundary Conditions

The respective GLT beams were modelled as four-layer beams made of individual lamella of Norway spruce (*Picea Abies*) placed together laterally. A schematic view of the models and the respective mesh used for the finite element model (FEM) is shown in Fig. 9, in which the local orientations of each lamella L, T, and R are aligned to the global coordinates X, Y, and Z directions. Thus, rhombic orthotropy has been assumed for the material law of timber. As in the empiric test setup the modelled beam was loaded in flatwise bending of the beams (i. e. edge-wise bending of the laminations).

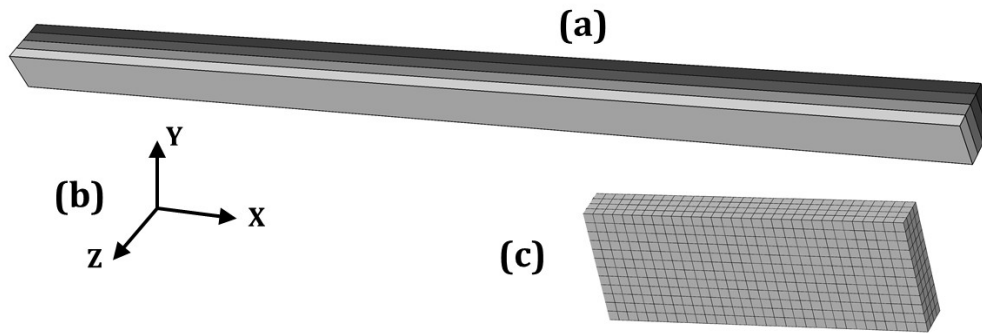


Fig. 9: Schematic views of the numerical model including: (a) a view of the GLT beam, (b) global coordinate system, and (c) a zoom in of the mesh

Simulations were done in two phases, primarily a moisture diffusion simulation was done to apply the gradients of Moisture contents (MC) to the model. It is worth noting, since there is not a moisture simulation module in Abaqus software, the heat transfer is used as the differential equations of moisture diffusion and heat transfer are mathematically similar and both use diffusive transport relations of Fick's law. The recorded data for relative humidity and temperature inside the testing hall were used in accordance with the Haliwood and Horrobin sorption isotherm model [12] to calculate the required moisture contents at the surface as input data for the boundary conditions for the moisture diffusion analysis.

Then, the output results of the primary phase were used as predefined fields to the second phase which deals with the mechanical deformation of the beams. For both phases, 3D brick elements are used, DC3D8 (8-node heat transfer brick) and C3D8 (8-node brick) elements, respectively. A mesh-sensitivity analysis was also performed to guarantee the accuracy of results in models with 77480 elements of 10 mm size. Additionally, to reduce the simulation runtime, a symmetry boundary condition was applied in the middle of the beams on the ZY plane. Additionally, the deformation measured right after the initial relaxation was taken as the reference value, defined as 100 % of the applied mid-span deflection ( $u_1 = 83.28$  mm for  $R_{\min} = 53$  m and  $u_2 = 61.28$  mm for  $R_{\max} = 72$  m). The time-dependent deflection was then derived from the experimental force–time data, slightly exceeding 100 % at the maximum recorded force assuming elastic behaviour during loading. After this brief initial phase, the deflection was kept constant at 100 %, and the corresponding reaction forces were evaluated based on the material's response to the evolving moisture conditions.

## 4.2 Numerical analyses results

The final contour of the central section of the modelled GLT beam is shown in Fig. 10. Fig. 11 presents a comparison of the moisture content changes at Point A (where in-situ MC in experiments was measured using the electrical resistance method at approximately 10 mm depth) against the values calculated from the Hailwood and Horrobin sorption isotherm model.

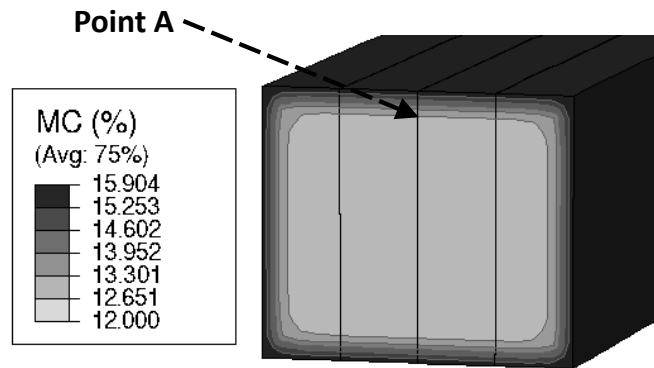


Fig. 10: Moisture content values on the central cross-section of the model shown on its latest contour

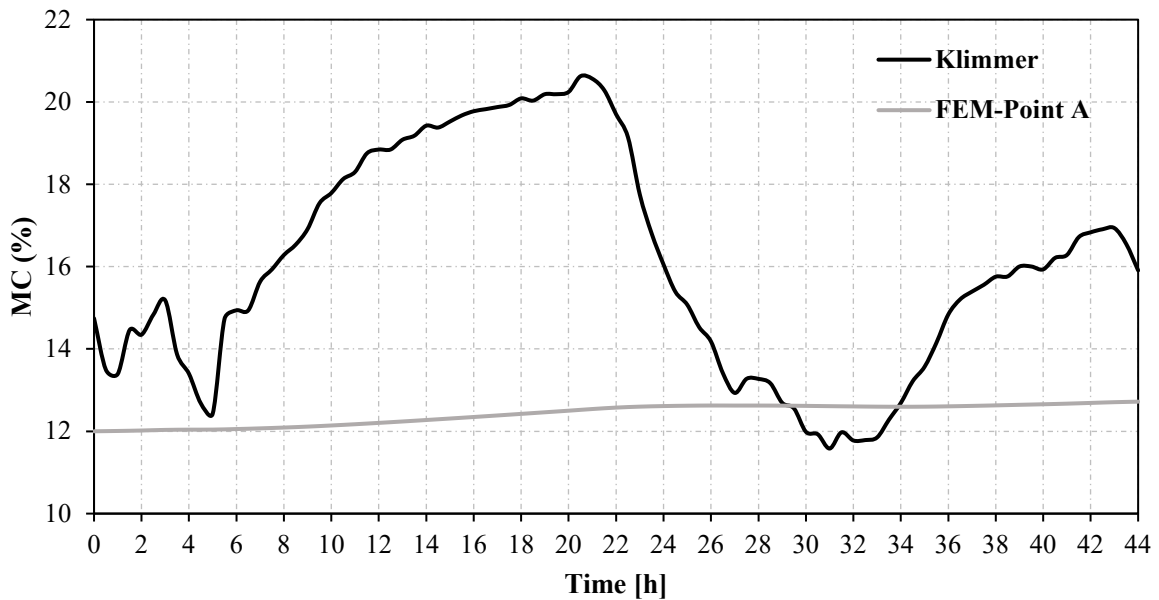
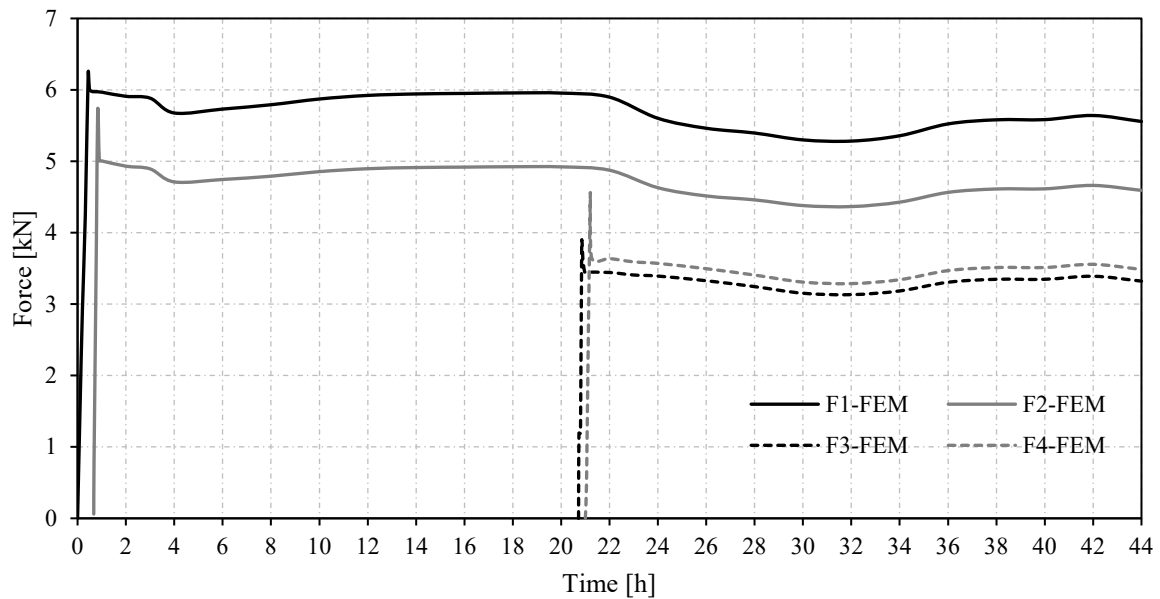


Fig. 11: Moisture content changes during the primary 44 hours simulation. Comparing the moisture contents calculated from the Hailwood and Horrobin sorption isotherm model (Klimmer) against the temporal values of moisture on point A shown in Fig. 10 (10 mm inside)

Then, the evolution of the forces during the primary 44-hour period is extracted from the simulations and shown in Fig. 12. The force graphs were extracted from points of interest close to the middle of the beams where symmetry boundary condition effects are diminished. These results follow a similar trend alike the experimental results with slightly more pronounced fluctuations, but still in a nice agreement of quantitative values (see Fig. 3).



*Fig. 12: force-time diagram of the relaxation test during the initial 44-hour period extracted from FEM simulations*

Afterwards, a new set of simulation were done, namely for long-term. Fig. 13 shows the long-term MC changes averaged on the model against the MC values calculated from the sorption isotherm model.

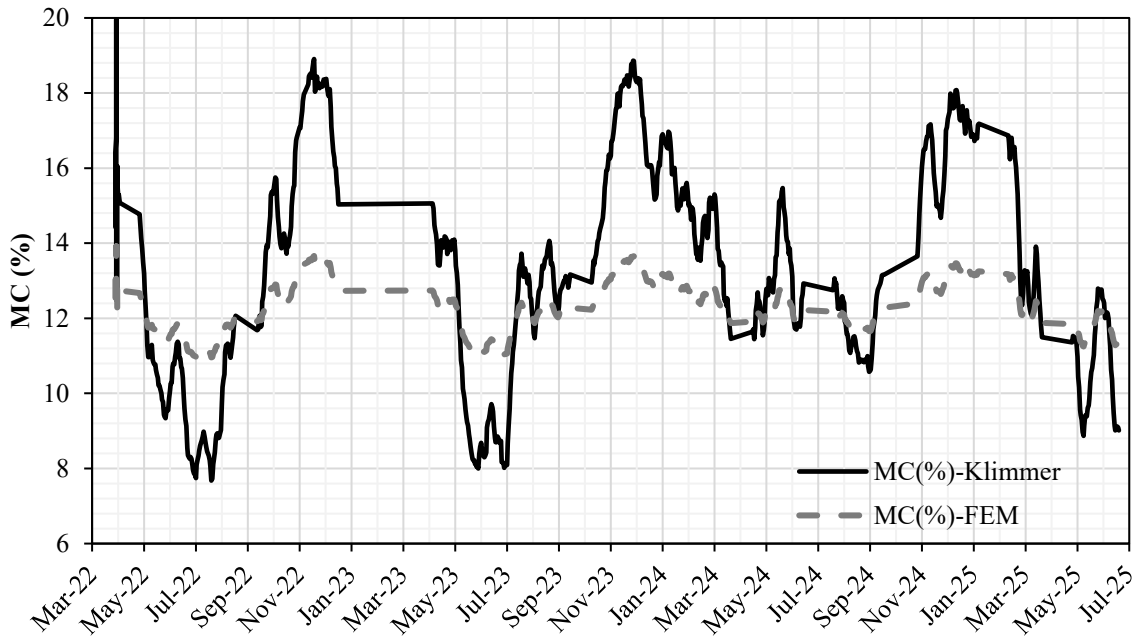


Fig. 13: Moisture content (MC) changes over long-term run, comparing the moisture contents calculated from the Haliwood and Horrobin (MC [%]-Klimmer) sorption isotherm model against the temporal average value of moisture on the whole FEM model (MC [%]-FEM)

The results obtained from this simulation could be compared with the experimentally recorded moisture contents using an electrical resistance device on some specific dates, shown in Table 5.

Table 5: Comparison of MC values between experimentally recorded data and values extracted from the long-term simulations for GLT beams against the average recorded values of MC in all four beams

Date	Experimental MC [%]	FEM MC [%]
6/28/2022	12.0	12.2
7/29/2022	11.6	11.3
9/7/2022	12.1	11.7
10/4/2022	12.7	12.4
11/18/2022	14.8	12.7
12/13/2022	14.6	14.1

Finally, the long-term mechanical simulations are performed to extract the evolution of forces in GLT beams. The results demonstrated in Fig. 14, show the simultaneous effects of stress relaxation with superimposed fluctuations caused by the seasonal MC changes. The final values of forces at the end of 38 months run highlight a reduction of 40 % and 37 % for the samples with the mid-span deflection of  $u_1 = 83.28$  mm (F1 and F2) and 45 % and 49 % for the samples with the mid-span deflection of  $u_2 = 61.28$  mm (F3 and F4).

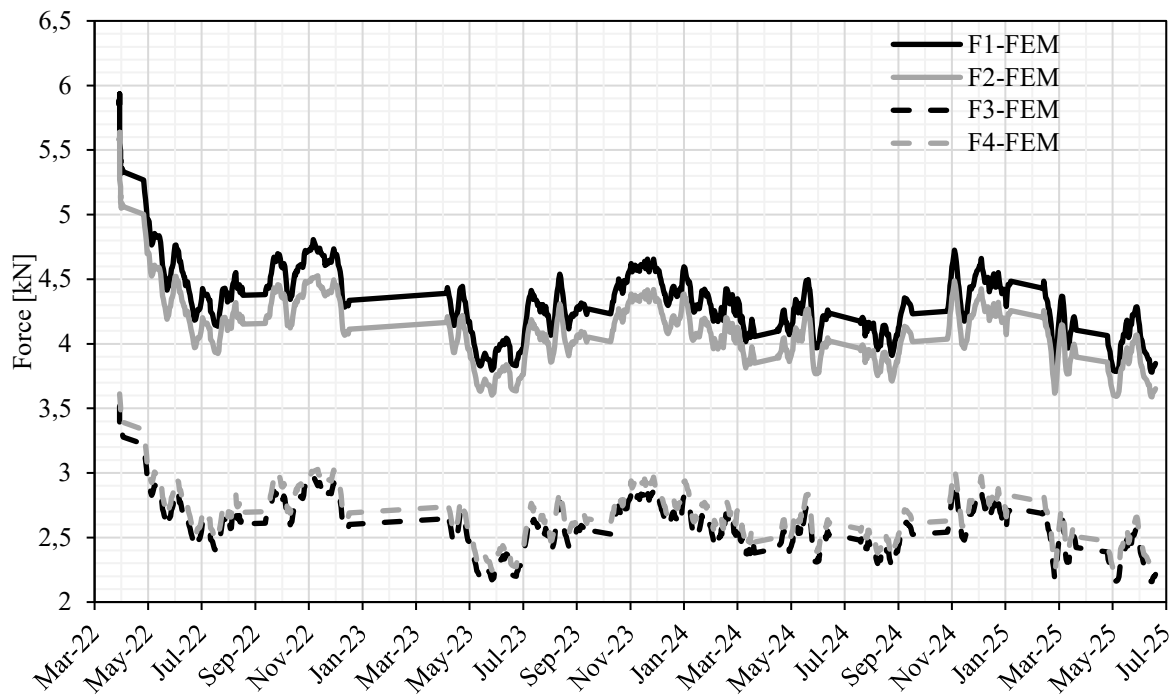


Fig. 14: force-time diagram of the relaxation test during the whole period of 3-year extracted from FEM simulations

## 5. COMPARISON OF EXPERIMENTAL RESULTS WITH NUMERICAL SIMULATION

The comparison between the experimental and simulated data across distinct temporal stages shows a good agreement for both short- and long-term phases, although the model parameters were not fitted to the empiric results, but very taken from literature values for the wood species Norway spruce. In the short-term phase (first 44 hours), the instantaneous elastic loading is given as input data adjusted from empirics and afterwards the corresponding reaction forces were validated based on the material's response to the transient moisture field. For the long-term assessment extending over 38 months as depicted in Figs. 15 and 16 for specimens F1/F2 and F3/F4, respectively, the simulation effectively reproduces the gradual reduction of internal forces due to stress relaxation, along with periodic fluctuations caused by variations in moisture content. These fluctuations align with the seasonal patterns recorded experimentally.

The “finger print” of the mechano-sorptive effects – implemented as part of the FE model – can clearly be recognised for the empiric and the simulation data on the scale of seasonal humidity / moisture cycles:

- Acceleration of relaxation during drying periods
- Reduction of relaxation during wetting periods
- Overall net effect of accelerated relaxation after a total cycle

The moisture diffusion results of the simulations are independently validated by comparing the MC values extracted from simulations against the direct measurements at specific time points (Table 5), showing nice correspondence.

The overall force reduction after 38 months, in specific for samples with mid-span deflection of  $w_2 = 61.28$  mm corresponds closely to the experimentally derived relaxation ratios, demonstrating both quantitative and qualitative consistency between experimental and numerical results.

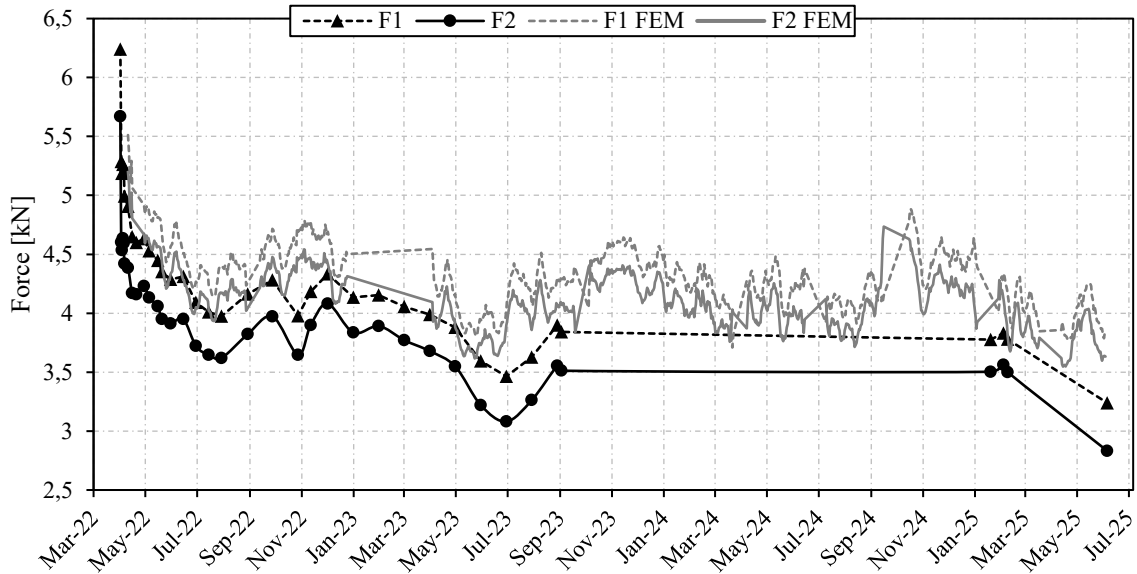


Fig. 15: force-time diagram of experimental and numerical data for specimens F1 and F2 ( $u1 = 83.28$  mm)

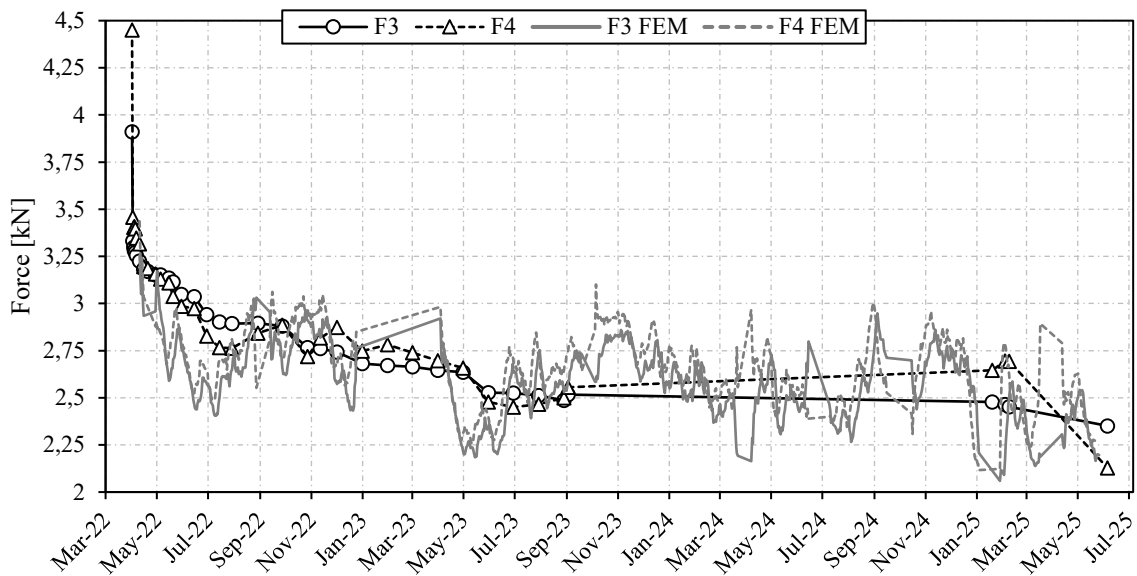


Fig. 16: force-time diagram of experimental and numerical data for specimens F3 and F4 ( $u2 = 61.28$  mm)

## 6. SUMMARY AND OUTLOOK

Long-term relaxation tests have been carried out with four pairs of Norway spruce GLT beams being subjected to constant bending deflections corresponding to two different mid-span deflections of  $u_1 = 83.28$  mm and  $u_2 = 61.28$  mm for a total time span of 38 months. The stress evolution of the beams was monitored by continuously measuring the reaction forces of the beams at mid-span. Force measurements were taken daily for 18 months straight and then again after 34 and 38 months. The beams stored in a not conditioned, naturally ventilated storage hall were exposed to changes in ambient temperature and humidity throughout the test period.

Following a significant relaxation of about 15 % within the first 24 h, the obtained time-dependent force relaxation curves subsequently display superimposed effects of viscoelastic and mechano-sorptive behaviour throughout. While overall the reduction of spring-back force appeared as gradual but consistent across the 38-month timeframe, moisture uptake and release during winter and summer periods, respectively, manifested notably in temporarily accelerated and retarded relaxation rates. Complementary FEM analyses incorporating an already established material model as well as the actual climate data of the test environment were able to replicate the observed relaxation behaviours closely. The compared simulation and empiric data both showed the typical pattern of mechano-sorptive effects yielding accelerated relaxation by the seasonal moisture cycles.

The reported investigations contain consistent insight into the expectable relaxation of internal stresses in timber elements induced by pre-bending. It should be noted here that moisture changes – as typical effects of the seasonal fluctuations at service class 2 conditions – contribute positively to a reduction of the stresses generated by initial bending in the GLT beams.

Besides the herein-discussed case of timber grid shells, such internal stresses are of major concern also in the production of curved GLT elements [13]. Furthermore, against the background of the rapidly growing possibilities of computational design in conjunction with semi-automated and CNC-based fabrication processes being now state-of-the-art in manufacture of engineered wood products, curved or bent wooden free-form structures steadily gain architectural interest. In order to safely design structurally complex scenarios featuring curved elements, knowledge about the time-dependent internal stress state can be paramount.

## REFERENCES

- [1] LARA-BOCANEGRA, A. J., MAJANO-MAJANO, A., ARRIAGA, F., GUAITA, M.: *Long-term bending stress relaxation in timber laths for the structural design of lattice shells*. *Constr. Build. Mater.* 193 (2018)
- [2] TAYEB, F., CARON, J.-F., BAVEREL, O., DU PELOUX, L.: *Stability and robustness of a 300 m<sup>2</sup> composite gridshell structure*. *Constr. Build. Mater.* 49 926–938, 2013
- [3] D’AMICO, B., KERMANI, A., ZHANG, H., PUGNALE, A., COLABELLA, S., PONE, S.: *Timber gridshells: numerical simulation, design and construction of a full-scale structure*, *Structures* 3 227–235, 2015
- [4] FREY, I.: *Wilhelma: Wann kommt Elefantenwelt statt Schaubauernhof?* *Stuttgarter Nachrichten*, 13.02.2025, online at: <https://www.stuttgarter-nachrichten.de/inhalt.wilhelma-elefantenwelt-schaubauernhof.c9aa9580-035a-4e71-b987-63f734202595.html> (last accessed on 26th of September 2025)
- [5] STREIB, D., AICHER, S., GAUSS, F., CAUSSARIEU, G., PETER, B.: *The timber grid shell of the new Elephant house at the zoological-botanical garden Wilhelma in Stuttgart – investigations on joint stiffnesses and capacities*. *Otto-Graf-Journal*, Stuttgart, 2022
- [6] EN 14080:2013: *Timber structures – Glued laminated timber and glued solid timber – Requirements*. European Committee for Standardization (CEN), Brussels, Belgium
- [7] TORATTI, T., SVENSSON, S.: *Mechano-sorptive experiments perpendicular to grain under tensile and compressive loads*. *Wood Sci Technol* 34 317–326, 2000
- [8] FORTINO, S., HRADIL, P., METELLI, G.: *Moisture-induced stresses in large glulam beams. Case study: Vihantasalmi bridge*. *Wood Mater Sci Eng.* 5 366–380, 2019
- [9] EN 1995-1-1: *Design of timber structures – Part 1-1: General Common rules and rules for buildings*. European Committee for Standardization (CEN), Brussels, Belgium, with corrections and amendments + AC:2006, A1:2008, and A2:2014’

- [10] D'AMICO, B., KERMANI, A., ZHANG, H.: *Form finding and structural analysis of actively bent timber grid shells*. Eng. Struct. 81 195–207, 2014
- [11] HASSANI, M.M., WITTEL, F.K., HERING, S., HERRMANN, H.J.: *Rheological model for wood*. Computer Methods in Applied Mechanics and Engineering 283, 2015
- [12] THYBRING, E.E., BOARDMAN, C.R., ZELINKA, S.L., & GLASS, S.: *Common sorption isotherm models are not physically valid for water in wood*. Colloids and Surfaces A: Physicochemical and Engineering Aspects 627, 2021
- [13] YU, T., KHALOIAN, A., VAN DE KUILEN, J.-W.: *Influence of the manufacturing process on the stress state of curved glulam beams*. Computers and Structures 316, 2025

